J. theor. Biol. (1997) **189,** 41–51

A Model for Cell Movement During *Dictyostelium* Mound Formation

TILL BRETSCHNEIDER*, BAKHTIER VASIEV† AND CORNELIS J. WEIJER†‡

* *Zoological Institute, University of Munich, Luisenstrasse* 14, 80333 *Munich, Germany, and the* † *Department of Anatomy & Physiology, Old Medical School, University of Dundee, Dundee DD*1 4*HN, UK*

(*Received on* 7 *January* 1997, *Accepted in revised form on* 3 *June* 1997)

Dictyostelium development is based on cell-cell communication by propagating cAMP signals and cell movement in response to these signals. In this paper we present a model describing wave propagation and cell movement during the early stages of *Dictyostelium* development, i.e. aggregation and mound formation. We model cells as distinct units whose cAMP relay system is described by the Martiel–Goldbeter model. To describe cell movement we single out three components: chemotactic motion, random motion and motion due to pressure between cells. This pressure results in cells crawling on top of each other and therefore to the extension of the aggregate into the third dimension. Using this model we are able to describe aggregation up to the mound stage. The cells in the mound move in a rotational fashion and their movement is directed by a counter-rotating spiral of the chemo-attractant cAMP. Furthermore, we show that the presence of two subpopulations with different inherent chemotactic velocities can lead to cell sorting in the mound. The fast moving cells collect into the centre while the slow cells occupy the rest of the mound. This model allows the direct comparison of the properties of the cAMP waves properties and movement behaviour of individual cells with experimental data. Thereby it allows a critical test of our understanding of the basic cellular principles involved in the morphogenesis of a simple eukaryote.

Introduction

Multicellular *Dictyostelium* development results from chemotactic aggregation of individual amoebae into a multicellular aggregate. During aggregation the cells differentiate into several prestalk cell types and into prespore cells (Williams, 1995; Early *et al*., 1995). These cells sort out chemotactically to form a standing slug in which the different cell types are arranged into a basically one-dimensional pattern. The slug can migrate under the influence of environmental signals like light, temperature and humidity to reach a place suitable to form a fruiting body (Loomis, 1982). The fruiting body consists of a stalk supporting a mass of spores. The prestalk cell types form the stalk, basal disk, upper and lower cup in the fruiting body while the prespore cells are the precursors for spores. Under suitable conditions the spores can germinate to release amoebae again.

Dictyostelium development occurs in the absence of food and the cells do not divide significantly during development (Loomis, 1982). Morphogenesis is the result of differentiation of vegetative amoebae into several cell types and differential chemotactic cell movement to put them in the right place (Williams & Jermyn 1991; Williams, 1995; Firtel, 1996). Our goal is to mathematically describe this morphogenetic process at the cellular level. Aggregation is relatively well understood, it results from wave propagation of the chemo-attractant cAMP and chemotactic cell movement (Alcantara & Monk, 1974; Tomchik & Devreotes, 1981; Gerisch *et al*., 1975). Adaptation of the cells after stimulation, most likely caused by receptor and G protein phosphorylation, ensures unidirectional (outward) wave propagation (Devreotes, 1989; Parent & Devreotes, 1996). The cells

‡ Author to whom correspondence should be addressed.
E-mail: C.J.Weijer@dundee.ac.uk.

0022–5193/97/210041 + 11 $25.00/0/jt970490

are chemotactically sensitive to the cAMP signal and move inwards in the direction of increasing cAMP concentrations. Since the cells detect periodic outward propagating waves, their movement is also periodic and inward directed (Cohen *et al*., 1971a,b; Alcantara & Monk, 1974). Inhomogeneities in cell density then lead to a symmetry breaking and formation of aggregation streams (Nanjundiah, 1973). There are various models that describe the cAMP relay kinetics as well as the formation of concentric and spiral waves when the cells are coupled by diffusion (Tyson *et al*., 1989a,b; Tang & Othmer, 1995). Models have been proposed which include chemotaxis and lead to stream formation showing that these processes are relatively well understood (Levine & Reynolds, 1991; Vasiev *et al*., 1994, Höfer *et al*., 1995, van Oss *et al*., 1996; Dallon & Othmer, 1996).

The later part of development however is less well understood. After stream formation the cells collect in the aggregation centre where they start to pile on top of each other and the aggregate becomes three-dimensional to form the mound. In the mound the cells are not motionless but move continuously in most strains in a rotational fashion. Their movement is directed by counter-rotating single or multi-armed spiral waves (Siegert & Weijer, 1995; Rietdorf *et al*., 1996). Another important event at this stage is the sorting of prespore and prestalk cells. Cells start to differentiate during late aggregation and enter the mound in a more or less random fashion and then sort out. Prestalk cells go to the top of the mound where they form a distinct structure, the tip, while the prespore cells stay, behind (Sternfeld & David, 1981a). The process of cell sorting is still poorly understood although it presumably involves differences in cell movement speed, cell adhesion and possibly cell type specific differences in cAMP relay.

The main difficulty in the theoretical description of later *Dictyotelium* morphogenesis is the description of cell movement in mounds and slugs, i.e. at high cell density. Two different solutions have been proposed. In one elegant approach the cells are modelled as discrete units covering many grid points. Movement is achieved by allowing the cells to change shape by covering different grid points (Savill & Hogeweg, 1997). Although interesting, this approach is still limited to computations involving only few independent cells. In a completely different approach the cells are considered as a compressible liquid which can move under the influence of chemotactic forces (Vasiev *et al*., 1997a). This formulation succeeds well in describing the overall motion of the cells during aggregation and at the mound stage, however it is much more difficult to include other relevant biological processes like random differentiation, cell sorting and differential cell movement of different cell types. Therefore, an alternative approach is being investigated. One possibility which comes to mind naturally and has been suggested previously (Kessler & Levine, 1993) is to treat the chemicals as continuous and cells as discrete with possibly different properties. The problem with this approach is to find reasonable descriptions for the movement of the cells as they reach high densities such as in the mound.

In the present paper we set out to develop such model using the Martiel–Goldbeter (Martiel & Goldbeter, 1987) description to model cAMP wave propagation (different components of the model can be readily associated with biologically relevant variables, i.e. receptors, their phosphorylation, cAMP synthesis by adenylyl cyclase and breakdown by cAMP phosphodiesterase) and automatons (Kessler & Levine, 1993; Vasieva *et al*., 1994) to model the cells. We show that in order to obtain movement of cells in the third dimension as well as simultaneous rotational movement we need local compaction and relaxation of cell density. Chemotactic motion results in a local cell density increase and the development of a density dependent pressure to its successive relaxation. Furthermore, we show that the model succeeds in producing a simple form of cell sorting of prestalk and prespore cells at the mound stage.

Model Description

In our model we represent cells as discrete entities (cells) which are able to emit cAMP signals, move and interact with each other. Each cell is defined by its individual list of properties so that it is possible to model different cell types, as well as random variations of certain parameters within each cell type.

The signalling system of each cell is described by the three variable Martiel–Goldbeter model (Martiel & Goldbeter, 1987). Three variables describe the change of extracellular cAMP (γ), intracellular cAMP (β) and the activation state of the cAMP receptors (ρ) over time.

$$\frac{\partial \gamma}{\partial t} = \left(\frac{k_t}{h}\right)\beta - k_e\gamma; \quad \gamma = \frac{[\mathrm{cAMP}]_{\mathrm{extracellular}}}{K_R}; \qquad (1)$$

$$\frac{\partial \beta}{\partial t} = q'\Phi(\rho, \gamma) - k_i\beta - k_i\beta; \quad \beta = \frac{[\text{cAMP}]_{\text{intracellular}}}{K_R}; \tag{2}$$

$$\frac{\partial \rho}{\partial t} = -f_1(\gamma)\rho + f_2(\gamma)(1-\rho);$$

$$\rho = \frac{[R]+[RP]}{[R]+[RP]+[D]+[DP]}; \tag{3}$$

$$\Phi(\rho, \gamma) = \frac{\lambda_1 + Y^2}{\lambda_1 + Y^2}; \quad Y = \frac{\rho\gamma}{1+\gamma};$$

$$f_1(\gamma) = \frac{k_1 + k_2\gamma}{1+\gamma}; \quad f_2(\gamma) = \frac{k_{-1} + k_{-2}c\gamma}{1+c\gamma};$$

The first equation describes the change in the level of extra-cellular cAMP, γ, over time. These changes occur due to the secretion of intracellular cAMP over the membrane and cAMP hydrolysis by phosphodiesterases outside the cell. The second equation defines the level of intracellular cAMP, β. It takes into account the synthesis of intracellular cAMP by adenylate cyclase in response to a cAMP stimulus, loss of intracellular cAMP due to secretion and intracellular hydrolysis. The last equation reflects changes in the state of receptors, ρ, binding cAMP at the cell surface. It defines the relative number of active receptors.

Cells are coupled by diffusion of the extracellular cAMP (γ). Therefore we include a diffusion term (Tyson *et al*., 1989a,b) and in addition a dependence of the production and decay of cAMP on cell density. We model a three-dimensional medium as consisting of three-dimensional volume elements (voxels). Each voxel (i, j, k) is characterized by a number of cells (N_{ijk}) and by the extracellular cAMP level (γ_{ijk}) in this voxel. We have modified eqn (1) as following:

$$\frac{\partial \gamma_{ijk}}{\partial t} = D\nabla^2\gamma_{ijk} + \sum_{n=1}^{N_{ijk}} \left(\left(\frac{k_t^n}{h} \right) \beta^n - k_e^n \gamma_{ijk} \right); \tag{4}$$

the index n denotes the nth cell in the voxel (i, j, k). So the change of the extracellular cAMP concentration (γ_{ijk}) in a voxel (i, j, k) is determined by the amount of cAMP that diffuses in/out, and by the cAMP produced and destroyed by all cells in this voxel. Diffusion of cAMP is assumed to take place in the aqueous surface of the substrate (plane $k = 1$) and in the volume of the aggregate. Therefore (1) has to be solved for every grid element where diffusion occurs. Equations (2) and (3) which describe the influence of γ_{ijk} on the intracellular cAMP level, β^n, and the state of the receptors, ρ^n are evaluated for each cell.

The cells' velocity $\mathbf{v}$ is assumed to consist of three components: chemotactic motion, $\mathbf{v_c}$; random motion, $\mathbf{v_r}$, and motion due to pressure, $\mathbf{v_p}$, so that to calculate cell coordinates, $\mathbf{x}$, we used the following equation:

$$\mathbf{x} = \mathbf{x_0} + (\mathbf{v_c} + \mathbf{v_r} + \mathbf{v_p})t; \tag{5}$$

To determine the number of cells, N_{ijk}, in each grid, the real coordinates of all cells are mapped to grid volume elements by $\mathbf{x} = [\mathbf{x}/\Delta x]$; the brackets indicate that only the integer part of the right hand side is considered.

Chemotaxis; cells move chemotactically in the direction of the extracellular cAMP gradient, $grad\gamma$, when $\partial\gamma_{ijk}/\partial t > k_{th} \cdot k_{th}$ was set to $0.5*10^{-7}$ M min^{-1} (Parnas & Segel, 1977, 1978) and, as a first approximation, the cell's speed is supposed to be constant and independent from the value of $grad\gamma$:

$$\mathbf{v_c} = k_{ch} * grad\gamma / |grad\gamma|; \tag{6}$$

We set $k_{ch} = 60\ \mu$m min^{-1}. This is much higher then the velocity of cells observed in experiments during aggregation which is about 15 μm min^{-1} (Alcantara & Monk, 1974; Siegert & Weijer, 1991) but is not so far from the speed measured in mounds (Rietdorf *et al*., 1996). The high value is needed to compensate for the short time cells move in the simulation (approx. 20 s per wave) in contrast to the *in vivo* situation [about 100 s (Alcantara & Monk, 1974) see discussion].

Random motion has been modelled as motion in a random direction where by the cells are shifted 0.16 μm every 10$^{\text{th}}$ time-step (1.3 s). This results in an average displacement of 1μm each minute.

Pressure provides a means to relax the temporary increase in cell density in tight aggregates, which results from the chemotactic motion of the cells towards the wave source. It is also responsible for the upward cell motion during mound formation.

We describe this pressure in one way by assuming an average cell density of 10^6 cells mm^{-3} in a tight aggregate. If the cell density exceeds this value a pressure develops which repels cells from this region. Cell density is measured as the number of cells per voxel and varies between 0 and 2. We set the space step equal to the size of one cell (grid volume element is $10 \times 10 \times 10\ \mu$m^3). If more than one cell happens to be in one voxel the cells move in the direction opposite to the cell density gradient with a mean velocity $|\vec{\mathbf{v}}_\mathbf{p}|$ of 9 μm min^{-1} for as long as the density is greater than one.

$$\mathbf{v_p} = -k_p * gradN/|gradN|. \quad (7)$$

We allow up to two cells per grid ($N_{ijk} < = 2$) which means that temporary compression is possible in a limited range.

The method described so far to calculate the pressure between cells is computationally fast but fairly coarse. The rule that a grid cannot contain more than two cells is rather ad hoc and results in a limited set of possible values for the density gradients. It results in cells stopping at the voxel boundaries. They cannot enter a grid which is already filled by two cells. Furthermore, if the density in a given voxel is greater than one, the cells will try to move out to voxels of lower density. However, as soon as they reach an empty voxel they will stop moving. These characteristics will lead to an accumulation of cells at the voxel boundaries. This can be improved in a second way to describe pressure by the use of a more accurate but computationally more laborious method. We introduce a continuous function to describe the repelling forces resulting from the interaction between cells. In this calculation we use the real coordinates of the cells and any possible effects of the discretisation of cell density are hereby avoided. Cell-cell interaction is described by a repelling force which acts when cells come closer than 10 μm. It decreases as $1/r^2$, where r is the distance between two cell centers. To calculate this force we consider all neighbouring cells that are located within 1 cell diameter (10 μm) of a particular cell (every time step). The velocity of the cell under consideration resulting from its interaction with a neigbouring cell is given by:

$$k_p\left(\frac{1}{|\mathbf{x}-\mathbf{x_n}|^2} - c\right)[\mu\text{m min}^{-1}]; \quad c = 0.01\ \mu\text{m}^{-2},$$

$$k_p = 3600\ \mu\text{m}^3\ \text{min}^{-1}$$

when $|\mathbf{x}-\mathbf{x_n}| < 10\ \mu$m, $k_p = 0$ if $|\mathbf{x}-\mathbf{x_n}| > 10\ \mu$m. With $|\mathbf{x}-\mathbf{x_n}|$ being the distance in μm between a neighbour cell with coordinates $\mathbf{x_n}$ and the cell of interest located at $\mathbf{x}$. The direction of motion $(\mathbf{x}-\mathbf{x_n}/|\mathbf{x}-\mathbf{x_n}|)$ is pointing away from the neighbour cell; The constant c ensures that the function is zero at a distance of one cell diameter.

For N interacting neighbouring cells we then have

$$\mathbf{v_p} = \sum_{n=1}^{N}\left(k_p\left(\frac{1}{|\mathbf{x}-\mathbf{x_n}|^2} - c\right)\frac{\mathbf{x}-\mathbf{x_n}}{|\mathbf{x}-\mathbf{x_n}|}\right); \quad (7a)$$

The first method to describe pressure was used in Figs 1–3 and 5, the second method was used in Fig. 4.

NUMERICAL SCHEMES

To calculate the gradient of γ we have used a central difference scheme.

$$grad\gamma = \begin{bmatrix} (\gamma_{i+1,j,k} - \gamma_{i-1,j,k})/(2*\Delta x) \\ (\gamma_{i,j+1,k} - \gamma_{i,j-1,k})/(2*\Delta x) \\ (\gamma_{i,j,k+1} - \gamma_{i,j,k-1})/(2*\Delta x) \end{bmatrix}; \quad (8)$$

where Δx is a value of space step. This simple scheme led to a pronounced stream formation in diagonal directions. We eliminated this anisotropy by alternating the direction used for computing the gradients in successive iterations. The alternative scheme evaluates the gradient in the diagonal directions:

$$grad\gamma = \begin{bmatrix} ((\gamma_{i+1,j+1,k} - \gamma_{i-1,j-1,k}) + (\gamma_{i+1,j-1,k} - \gamma_{i-1,j+1,k}))/4*\Delta x) \\ ((\gamma_{i+1,j+1,k} - \gamma_{i-1,j-1,k}) - (\gamma_{i+1,j-1,k} - \gamma_{i-1,j+1,k}))/4*\Delta x) \\ (\gamma_{i,j,k+1} - \gamma_{i,j,k-1})/(2*\Delta x) \end{bmatrix}; \quad (9)$$

The same procedure has been used to calculate *gradN* in (7).

Diffusion of extracellular cAMP, γ, takes place in the plane $k = 1$ (the aqueous surface of the substrate) and at grid points (i, j, k) $(k > 1)$ where $N_{ijk} > 0$. For the evaluation of the diffusion term we used the following scheme:

$$\begin{aligned} \nabla^2\gamma = (4(&\gamma_{i+1,j,k} + \gamma_{i-1,j,k} + \gamma_{i,j+1,k} + \gamma_{i,j-1,k} + \gamma_{i,j,k-1} \\ &+ \gamma_{i,j,k-1}) + \gamma_{i+1,j+1,k} + \gamma_{i-1,j+1,k} + \gamma_{i+1,j-1,k} + \gamma_{i-1,j-1,k} \\ &+ \gamma_{i+1,j,k+1} + \gamma_{i+1,j,k-1} + \gamma_{i-1,j,k+1} + \gamma_{i-1,j,k-1} \\ &+ \gamma_{i,j+1,k+1} + \gamma_{i,j+1,k-1} + \gamma_{i,j-1,k+1} + \gamma_{i,j-1,k-1} \\ &- 36\gamma_{i,j,k})/8\Delta x^2) \end{aligned} \quad (10)$$

We allow no fluxes of cAMP (γ) at the boundary of the aggregate and at the boundary of the medium. As cells cannot penetrate the substrate they are not allowed to move to the plane $k = 0$. To be able to calculate the vertical cell density gradients on the substrate ($k = 1$) we used an additional plane ($k = 0$) where the cell density N_{ijk} reflects that in the plane $k = 1$. This takes into account the no flux boundary conditions (downward) for the cells on the substrate and allows the calculation of the upward gradients.

MODEL PARAMETERS

The Martiel–Goldbeter model was used by Tyson *et al*. (1989b) to simulate the propagation of cAMP waves in a continuous medium. Our model however deals with a heterogeneous distribution of cells. Therefore, production and decay of cAMP are considered to take place only at grid points containing cells ($N_{ijk} > 0$). In order to obtain good streaming patterns formed by moving cells we have modified Tyson's set of parameters to the following: $K_R = 10^{-7}$ M, $k_1 = 0.12\ \text{min}^{-1}$, $k_{-1} = 1.2\ \text{min}^{-1}$, $k_2 = 2.22\ \text{min}^{-1}$, $k_{-2} = 0.011\ \text{min}^{-1}$, $k_i = 3.3\ \text{min}^{-1}$, $k_t = 3.0\ \text{min}^{-1}$, $k_e = 120.0\ \text{min}^{-1}$, $h = 0.125$, $D = 0.01\ \text{mm}^2\ \text{min}^{-1}$, $q' = 3800.0$, $l_1 = 0.0001$, $l_2 = 2.4$, $c = 10.0$. This set of parameters results in a strong dependence of wave propagation speed on cell density which has been shown to be necessary for stream formation (Levine & Reynolds, 1991).

The spatial domain used for the simulations of aggregation (Fig. 1) consists of $100 \times 100 \times 20$ voxels. To model aggregation we start with 3000 cells randomly distributed on the bottom plane ($k = 1$) of this volume, so that the initial cell density is $3*10^5$ amoebae cm^{-2}, which agrees with standard experimental conditions. The *in vivo* threshold below which no waves can propagate is $5*10^4$ amoebae cm^{-2} (Konijn & Raper, 1961; Konijn, 1968; Hashimoto *et al*., 1975, Mato *et al*., 1975).

The integration method used is an explicit Euler time stepping. We have checked the numerical stability by variation of the space and time steps and we have used $\Delta x = 0.01$ mm $\Delta t = 0.13$ s. These values give stable and accurate results. The programs were written in standard C and the data were visualized using the Data Explorer program from IBM.

Results

DEVELOPMENT FROM SINGLE CELLS TO MOUNDS

Figure 1 shows a time series of aggregation and mound formation. The initial situation can be seen in Fig 1(a). Three thousand cells are placed randomly in the bottom plane ($1\ \text{mm}^2$) of a three-dimensional field. A cAMP spiral is initialized with initial period of rotation equal to 2.7 min and wave propagation speed about $250\ \mu\text{m}\ \text{min}^{-1}$. The frequency of spiral wave rotation increases in time, it is caused by the increase in cell density (van Oss *et al*., 1996), while the velocity of cAMP waves slightly decreases due to dispersion (Tyson & Keener, 1988). The spiral wave of cAMP causes cells to move into the direction of the spiral core. After about 10 waves of cAMP spiral wave rotation streams start to form [Fig. 1(b)]. Streaming occurs due to an instability which arises when cAMP production is strongly dependent on cell density (Levine & Reynolds, 1991). This density dependence leads to local speeding up of the waves in regions of high cell density resulting in turn in the attraction of even more cells to these regions (positive feedback). A transient ring of cells surrounding a cell-free hole forms at the aggregation centre. The radius is determined by the size of the spiral core which is characterized by a low cAMP level. The cells move out of the core region and try to collect on the trajectory described by the spiral tip. With increasing cell density at the aggregation centre the medium becomes more excitable. This results in a shrinking of the core region in time and to a contraction of the ring. Over time the streams become more pronounced. As aggregation continues the cell density at the aggregation centre increases more and more. Cells from the periphery that keep on heading for the centre exert pressure on cells in the very centre. The only possibility to reduce this pressure is upward motion of cells since downward motion is inhibited by the substratum. The result is the formation of a

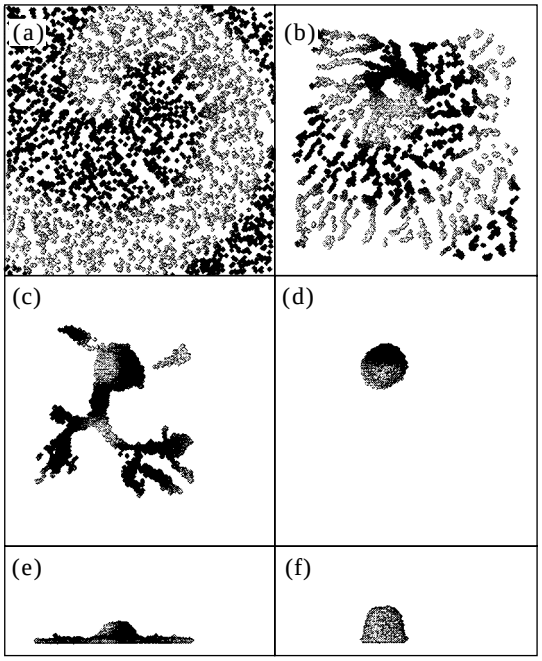

FIG. 1. Development of *Dictyostelium* from single cells to the mound stage. (a–d): top view of successive images of aggregation; (e, f) side view of the aggregates shown in (c, d). Cells are shown as dark spots on a white plane. The grey level of the cells shows the concentration of extracellular cAMP at their location (higher cAMP levels correspond to lighter colours). Initially 3000 cells have randomly been distributed on the first plane of the computational three-dimensional medium (a). At $t = 3.6$ hr (10^5 time steps) all cells have collected into one aggregate with diameter ca. 170 μm, height 130 μm.

mound [Fig. 1(c)]. Finally all cells collect in the aggregate of about 170 μm in diameter [Fig. 1(d)]. In the mound the period of the cAMP wave has decreased to 1.8 min.

As mound formation is the result of collective movement of single cells it depends very much on the rules for cell motion. The following section gives an overview of the influence of chemotaxis and random motion on aggregate formation and demonstrates the necessity to include a pressure mechanism to make cells move up into the third dimension.

Chemotactic motion

Figure 2(a) describes what happens if cells only move chemotactically. Streams form as seen in Fig. 1(b), but aggregation fails to proceed as the cell density in the aggregation centre becomes too high. The final structure obtained is a static monolayer of tightly packed cells. No more cells can enter the aggregation centre as the cell density in the centre cannot exceed the threshold of two cells per grid. The reason for assuming this threshold is that if it would not exist, all cells would finally come together in an aggregation centre with infinite cell density. Chemotactic motion alone therefore provides no means for extending the aggregate up in the third dimension. This can be demonstrated more clearly by looking at the movement of single cells. The tracks of nine cells during aggregation are shown, the starting point is indicated by a circle. The final points of the cell tracks remain quite far apart which means most of the cells stop before reaching the aggregation centre. The cAMP signal perceived by one of the cells over a period of 8 min corresponding to three periods of spiral wave rotation is shown in Fig. 1(a), right part, dashed line and its velocity as a solid line (calculated as the displacement of a cell over 10 iterations). The instantaneous velocity should give a rectangular curve as the cells move with a constant velocity. Deviations from the rectangular curve are due to changes in the direction of movement. Note that the cell is moving only during the rising phase of the cAMP wave which is in this case a very short period (less than 25 s).

Chemotactic and random motion

It is well known that cells which are not chemotactically stimulated still show some movement. They are not motionless in the absence of a signal as in the above calculation. It might even be expected that a certain degree of random motion might overcome some of the difficulties observed above. To investigate this in more detail we added random motion to the chemotactic motion [Fig. 2(b)].

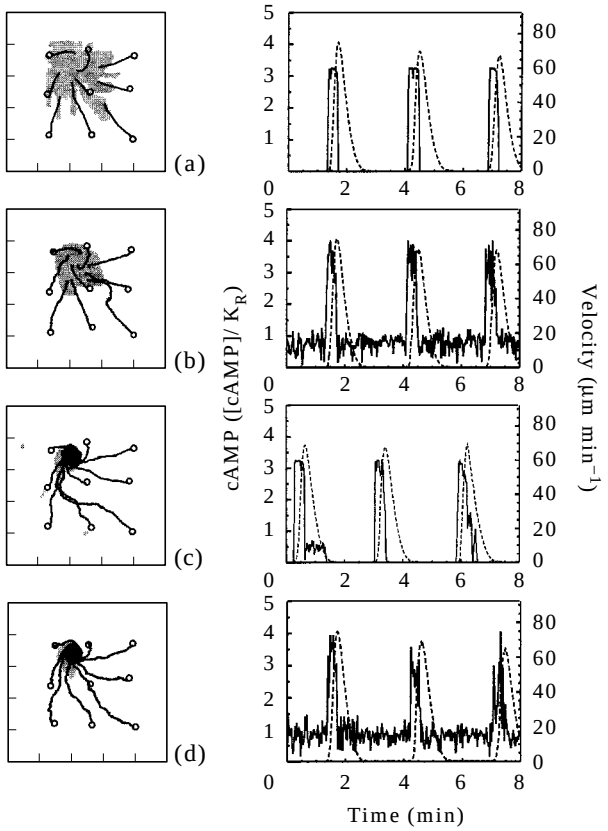

FIG. 2. Four different versions of the model are compared, i.e. chemotaxis only (a); chemotaxis plus random motion (b); chemotaxis plus pressure (c); all three components (d). Left column: top view of the final aggregates and cell tracks. The initial conditions are the same as in Fig. 1. The grey shaded area (in left column) outlines the structure obtained in 10^5 time steps (3.6 hr). In (a, b) it is a monolayer of cells with a cell density of two cells per grid; in (c, d) it is a three-dimensional structure similar to that in Fig. 1(d). The black lines show trajectories of arbitrary chosen cells whose initial location is denoted by a circle. Right column: extracellular cAMP (dashed line) and velocity (solid line) of a typical cell vs, time. Velocity profiles (right column) are drawn using cell displacement over subsequent 1.3 s time intervals (10 time steps).

The overall effect of random motion is that the protuberances seen in Fig. 2(a) vanish. Random motion smoothes the shape of the final aggregate. The final structure is almost a round two-dimensional disk [Fig. 2(b)]. The cell tracks show that the right bottom cell that got stuck previously in Fig. 2(a) now moves in closer to the aggregation centre. Note that random motion does not result in an extension of the structure into the third dimension. In the cell velocity profile random motion appears as a noise.

Chemotactic motion plus pressure

Now we introduce a mechanism that results in upward motion of cells. The higher the average cell

density in the aggregation centre becomes, the higher the probability that two cells share one voxel. In the preceding section aggregation came to an end when the cell density had reached two cells per grid everywhere in the aggregate. Here we assumed a pressure to be generated when the cell density exceeded one cell per grid, resulting in a movement of cells to regions of lower cell density. The global effect is that the average cell density in the aggregate is kept less than two cells per grid. With increasing cell density at the aggregation centre a cell cannot move any longer in the horizontal plane when it is completely surrounded by neighbouring cells as was shown in Fig. 2(a). Pressure makes it move up, since downward motion is inhibited by the substratum. The final aggregate shown in Fig. 2(c) is a three-dimensional mound [similar to Fig. 1(d)]. It is also seen that the cells continue to move in the aggregate. All tracks now end in some small neighbourhood [in Fig. 2(c) three-dimensional tracks are mapped to one plane] and aggregation is completed. A close look reveals however that not all cells are able to keep up with aggregation. Some clumps of cells (small grey spots) remain outside the main aggregate. A velocity profile of a cell just entering the mound is shown. It is seen that initially the cell is moving chemotactically for 25 s followed by a period of slower movement caused by pressure relaxation. The latter response deteriorates in about 30 s.

Chemotactic, random and pressure dependent movement

Finally all components together were taken into account. The final result [Fig. 2(d)] does not differ very much from that shown in Fig. 2(c). Random motion does not seem to have major consequences for mound formation but it still improves aggregation, all cells enter the aggregate.

Now let us compare cell movement in the various stages of aggregation by examination of the cell tracks at higher magnification. Figure 3(a) shows tracks of aggregating cells before mound formation, and Fig. 3(b) shows the tracks of cells in a mound. Figure 3(c) shows the beginning of the track of the yellow cell in Fig. 3(a). Figure 3(d) shows the track of the yellow cell in Fig. 3(b). Figure 3(e) and (f) show the corresponding velocity plots. In Fig. 3(c) the periods of chemotactic activity can be seen as straight lines, whereas periods when cells are only moving randomly appear as nodes (beads on a thread). The shift per wave is about 15 μm, the maximum velocity is up to 80 μm min^{-1} [Fig. 3(c)], the period is about 3 min. Cells move in a stop and go fashion with the go period lasting 25 s. The tracks in Fig. 3(d) again show a straight forward movement when the cell is moving chemotactically as in Fig. 3(c), with the direction a little more inward than the tangent on a circle. If a cell was not hindered by other cells in its inward movement it would go to the very centre on a spiral trajectory. At the end of the chemotactic movement phase and during a short time thereafter the developing pressure forces the cell to move outward. This results in movement on a closed circle on average. Random motion still takes place (beads on a thread picture).

Looking at the velocity [Fig. 3(f)] there are no major differences when compared to Fig. 3(e). With an increase in excitability of the medium due to a higher cell density the period decreases to 2 min. Obviously there is a big discrepancy between our model and experimental findings concerning cell movement in mounds. Cells move continuously and their velocity does not change in time very much as in our model. The result clearly demonstrates the necessity of including further interaction between the cells which will be discussed later.

Refinement of the model

The constraint of allowing only up to two cells per voxel results in temporal lingering of the cells at the voxel boundaries [Figs 3(c) and (d)]. To avoid this influence of the cell density discretisation on cell motion, we have explored a different approach to model cell-cell interactions. These interactions are described as a continuous function of the distance between cells. If the distance (r) between two cell-centres becomes less than 10 μm a repelling force develops proportional to $1/r^2$ which results in the cells moving away from each other. This refined but computationally more intensive description of cell-cell interactions results in a better description of cell motion in the mound and does not require the arbitrary restriction for the number of cells per voxel any more. Furthermore, the shape of the mound improves since the cells no longer linger at the grid boundaries as shown in Fig. 4.

Figure 4(a) shows a cross-section of a mound. The cAMP spiral wave is black, rotating clockwise. The arrows represent the cells' direction of motion. The colour indicates their speed (blue: low; green: high). Chemotactically moving cells in the front of the wave (green arrows perpendicular to the wave front) tend to move to the centre of the mound whereas cells in the back of the wave move outwards. This figure clearly illustrates the mechanism of cell movement in the mound. It results from rapid compaction during the rising phase of the wave followed by a slower relaxation of the density. This can also be seen in the

cell track in Fig. 4(b) (without random motion). The track is colour coded to indicate the extracellular cAMP values (blue: low; red: high) seen by the cell during its motion through eight successive waves. It can be clearly seen that the cell starts to move inwards during the rising phase of the waves followed by a period of outward directed movement during the relaxation of the pressure [also seen in Fig. 3(d)]. The density distribution in the mound shown in Fig. 4(a) is given in Fig. 4(c) (blue: 0 cells voxel^{-1}; red: 5 cells voxel^{-1}; mean density: 1.7 cells voxel^{-1} calculated for the whole mound). In the region of the wavefront the cell density is lower as average (light blue: 1 cell voxel^{-1}), whereas in the wave back the cell density temporarily increases to up to 5 cells voxel^{-1}. Pressure results in relaxation of the cell density, until the average density is reached again. Since cell motion is now completely independent of any grids the overall mound shape has also improved. The mounds are more hemispherical [Fig. 4(d)] rather than cylindrical as previously Fig. 1(f)].

CELL SORTING

Since one of the main future goals of this model is to investigate the mechanisms controlling cell sorting we have tested whether the basic mechanism for cell sorting could involve differences in movement efficiency of prestalk (PST) and prespore (PSP) cells (Early *et al*., 1995, Fig. 5). In our model we consider a higher chemotactic velocity for PST cells. PST cells are assigned a velocity of 40 μm min^{-1}, PSP—20 μm min^{-1}. In addition, PST are assumed to be more sensitive to cAMP (Matsukuma & Durston, 1979; Sternfeld & David, 1981a). We set the threshold value for PSTs chemotactic motion to zero, $k_{th} = 0$, i.e. they can detect any temporal changes in cAMP. Figure 5 shows the distribution of PSP and PST cells after 1 hr simulation time beginning from a random distribution of cells of both types inside the hemispherical mound. The PST cells have gathered in a central cylinder of the mound [Figs 5(b) and (c)]. It is clear that the fast moving cells sort to the middle but do not move up. Figure 5(d) shows the trajectories of a PSP and a PST cell that were originally neighbours. Their starting positions are in the periphery of the mound in the plane $z = 4$. While the PSP cell (green) moves on a circular trajectory almost returning to its starting point, the PST cell (yellow) heads to the centre. It finally ends on a circular trajectory with a very small radius. Figure 5 clearly shows that our model can produce some form of cell sorting and should therefore be useful in its further characterization.

Discussion

The model proposed in this paper is a first step towards a rigorous description of the cellular basis of morphogenesis. The approach to model the chemicals as continuous variables produced and destroyed by discrete entities, cells (which may differ in their kinetics and relatively simple rules to describe their movement) has been shown to be able to describe the essential behaviour of the cells during aggregation and mound formation. It can describe the organization of cells by self organizing propagating spirals, the assembly of cells into aggregation streams as well as the formation of a three-dimensional structure, the mound. The most important progress made by this description is the possibility for cells to move under conditions of close packing in the mound. Since our aim is to understand morphogenesis at the cellular level we need a description of morphogenesis at this level, i.e. at the level of the behaviour of single cells. We have designed our model such that we have access to those properties of the cells during the model calculations that allow a direct comparison with experimentally obtained and obtainable data. A qualitative and finally quantitative comparison of these data is the only way to evaluate the quality of the model to describe development.

Waves have been visualized during aggregation by fluorography of radio-labelled cAMP as well as by recording of the propagation of the associated darkfield waves. In the later stages of development direct measurement of cAMP has been proven to be impossible until now but it has been possible to record the propagation of optical density darkfield waves as well as a detailed analysis of the tracks and kinetics of cell movement in mounds (Siegert & Weijer, 1995; Rietdorf *et al*., 1996, 1997). In the slug and culmination stages of development it has not even be possible to measure darkfield wave propagation but it has been possible to analyse cell movement. Therefore, in this model we have concentrated on the analysis of the wave propagation and cell movement.

The model succeeds in describing wave propagation and cell movement during aggregation. The formation of aggregation streams is now relatively well understood and fulfills a minimal requirement for the model to achieve. Both the shape of the waves and the tracks of the cells in aggregation streams are at least qualitatively in agreement with experimental data. In the mound stage it is seen that the cells can move while being organized by a single counter rotating spiral. This is at least compatible with the very simplest phenomena observed in mounds. The movement of the cells is made possible by allowing

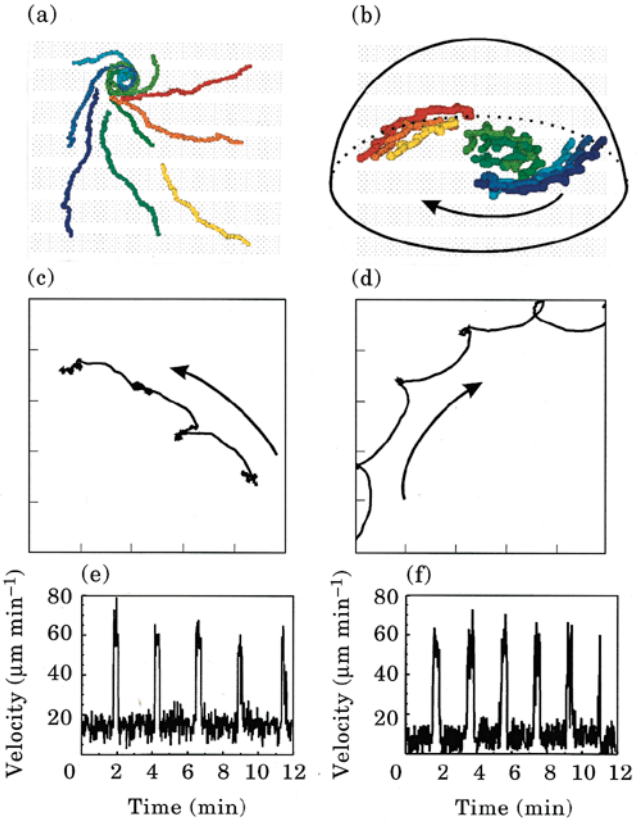

FIG. 3.

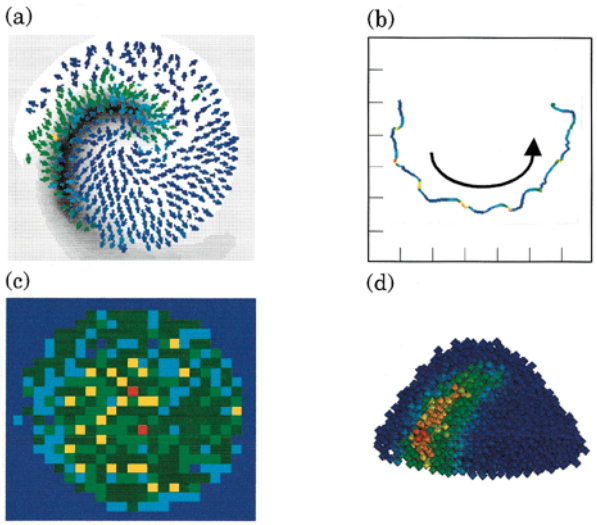

FIG. 4.

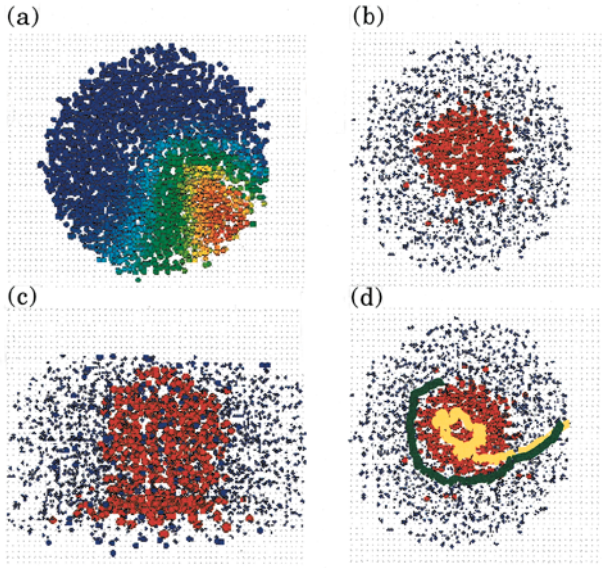

FIG. 5.

FIG. 3. (a, b) View of typical trajectories of cells in aggregation streams and in a mound. During early aggregation the cells move more less straight into the direction of the aggregation centre (a). The closer they come the more the tracks become curved. In the mound they move in a rotational fashion (b). (c, d) Tracks of the cells marked by a black arrow in the corresponding picture above at high magnification. The length of the x and y axis is 50 μm, the period of cell movement decreases from 2.7 min (e) to 1.8 (f).

FIG. 4. A refined model for cell cell interactions. (a) Cross-section of a mound: the cAMP concentrations are shown as grey values, black is high cAMP, the cells' velocities are shown as arrows; green: high velocity due to chemotactic motion, blue: low velocity. (b) The track of a cell in the centre of the mound during the passage of eight waves. The colour of the track represents the cAMP concentration detected by the cell during chemotactic motion. It changes from blue (low concentration) to red (high). The arrow indicates the direction of motion. The distance between the bold ticks on the axis represent 10 μm. (c) Density distribution corresponding to the cAMP distribution shown in Fig. 4(a) dark blue: 0, light blue: 1, dark green: 2, light green: 3, yellow: 4, red: 5 cells per voxel ($10 \times 10 \times 10$ μm). In the region of the wavefront the cell density is lower, in the back of the wave it is higher than the mean average of 1.7 cells per voxel. (d) The overall shape of the mound is more hemispherical as compared to the mound in Fig. 1(d).

FIG. 5. Cell sorting. (a) Top view of a mound. The cells' colour indicate the extracellular cAMP concentration (blue: low, red: high). (b, c) Top and side view showing the distribution of prestalk (red) and prespore (blue) cells. (d): examples of trajectories of a PST (yellow) and PSP (green) cell plotted over Fig. 5(b). Initially, 3000 cells have evenly been packed in a hemisphere (radius 90 μm, density: 1 cell per voxel) resembling a mound. 20% of cells are randomly chosen to represent prestalk cells, which are faster ($k_{ch} = 40\,\mu\text{m min}^{-1}$ for prestalk and $k_{ch} = 20\,\mu\text{m min}^{-1}$ for prespore cells) and more sensitive to chemotactic signals ($k_{th} = 0\,\text{M min}^{-1}$ for PST and $k_{th} = 0.5{*}10^{-7}\,\text{M}^{-1}$ for PSP). All other parameters are the same as in Fig. 1. The images shown represent the situation after 1 hr ($3{*}10^4$ time steps) of simulation.

(facing p. 48)

small density fluctuations at the mound stage. The cells compact locally during the rising part of the wave as a result of cAMP induced chemotaxis. This increase in density leads to a local pressure increase which due to a density dependent relaxation evens out in time thus resulting in cell movement in mounds.

We presented two methods for calculating the interaction between cells. The first one using gradients in cell density is fairly coarse. Nevertheless, it is capable of describing the effects of pressure adequately in that it results in upward motion of cells as well as movement of the cells in mounds. However, due to the discretisation of the cell-cell interaction there is a tendency for the cells to linger at the grid boundaries and the density of the cells is therefore higher around the gridlines and the shape of the mound is somewhat cylindrical. The advantage of this method is that it results in relatively fast computations. A more accurate description using a continuous function to describe cell-cell interactions was shown to improve the cell tracks and the overall shape of mounds. A continuous function for the interaction between cells furthermore has the advantage that the effects of other cell-cell interactions such as adhesion can be included more easily. An extension of this model to include cell adhesion and its role in the process of cell sorting is in preparation.

Closer examination of the trails show, however, that the cells in the mounds still move in a periodic fashion similar to the mode of movement during aggregation. This is not in agreement with the experimental data. The experimental data show that the cells in the mound as well as in aggregation streams move continuously with little periodic fluctuations on top (Rietdorf *et al*., 1996). This has been taken to imply that there are very strong cell-cell interactions, which make the mound behave mechanically more like a very viscous fluid (Vasiev *et al*., 1997a). To take this aspect into account the model will have to be extended in the future by inclusion of cell-cell adhesion which up to now has been neglected. Initial trials to include these interactions via coupling the velocity of cells by a velocity diffusion term so far have failed since they rapidly induced numerical instabilities in the system. Alternative approaches to model cell-cell interactions are still under investigation since this is an aspect that will be needed later on in the full description of morphogenesis where cell type specific cell-cell adhesion is known to play an important role.

The other observation made is that the geometry of the spiral does not change in the calculations as much as suggested in part by the experimental data. It is known that the frequency of the oscillations increase from 6 min to 2 min while wave propagation speed decreases from $600\,\mu\,\mathrm{min}^{-1}$ to $100\,\mu\,\mathrm{min}^{-1}$ leading to a 15-fold decrease in spiral wave length (Siegert & Weijer, 1989, 1991). This is in part the result of the increase in density during aggregation as well as in the feedback of the cAMP pulses on the expression of the components of the cAMP relay system (Tyson & Keener, 1988, Devreotes, 1989; Levine *et al*., 1996), leading to a big increase in cAMP receptors and cyclase during development. This is complicated furthermore by the expression of a series of different cAMP receptors in a cell-specific manner later in development (Chen *et al*., 1996; Firtel, 1996). These receptors show a progressive decrease in affinity for cAMP in order of their expression. This has been neglected at the moment. However, it has been suggested recently that this might be responsible for the formation of multi-armed spirals at the mound stage (Vasiev *et al*., 1997b) as well as for the development of more and less excitable cells leading to the formation of scroll waves in the tip and planar waves in the base of the slug (Steinbock *et al*., 1993; Bretschneider *et al*., 1995). These are all properties which are now under study and will be included in more refined versions of the model. Furthermore, it will ultimately be necessary to include a cell type proportioning mechanism which uses, in part, the cAMP signalling system to proportion the cell types and stabilize their differentiation state once they sort out (Schaap *et al*., 1996).

Despite some of the above-mentioned obvious limitations of the model we have shown that such a model can also be used to investigate the conditions which lead to cell sorting. By assuming that the prestalk and prespore cell types differ in their movement properties (Early *et al*., 1995) we have shown that it is possible to obtain cell sorting of the faster moving cells to a central core in the mound. Once the cells have sorted to the centre they will stay there. The cells will not sort to the top of the mound even under conditions where there is an overall asymmetry by allowing cAMP to diffuse in the agar which leads to lower cAMP levels in the base as in the top. It is clear that something else is needed. It also seems plausible from our preliminary calculations that another important requirement is a difference in excitability between the fast and slow moving cell types together with possibly yet another external asymmetry (e.g. oxygen; Sternfeld & David, 1981b) which leads to higher excitability of the cells on top compared to the cells in the base.

This work was supported by the Forschungsgemeinschaft (We 1127).

REFERENCES

Alcantara, F. & Monk, M. (1974). Signal propagation during aggregation in the slime mould *Dictyostelium discoideum*. *J. Gen. Microbiol*. **85**, 321–334.

Bretschneider, T., Siegert, F. & Weijer, C. J. (1995). Three-dimensional scroll waves of cAMP could direct cell movement and gene expression in *Dictyostelium* slugs. *Proc. Natl. Acad. Sci. U.S.A*. **92,** 4387–4391.

Chen, M. Y., Insall, R. H. & Devreotes, P. N. (1996). Signaling through chemoattractant receptors in *Dictyostelium*. *Trends Genet*. (*TIG*) **12,** 52–57.

Cohen, M. H. & Robertson, A. (1971a). Wave propagation in the early stages of aggregation of cellular slime molds. *J. theor. Biol*. **31,** 101–118.

Cohen, M. H. & Robertson, A. (1971b). Chemotaxis and the early stages of aggregation in cellular slime molds. *J. theor. Biol*. **31,** 119–130.

Dallon, J. C. & Othmer, H. G. (1997). A discrete cell model with adaptive signalling for aggregation of *Dictyostelium discoideum*. *Phil. Trans. R. Soc. Lond. B* **352,** 391–417.

Devreotes, P. N. (1989). *Dictyostelium discoideum*: A model system for cell-cell interactions in development. *Science* **245,** 1054–1058.

Early, A., Abe, T. & Williams, J. (1995). Evidence for positional differentiation of prestalk cells and for a morphogenetic gradient in *Dictyostelium*. *Cell* **83,** 91–99.

Firtel, R. A. (1996). Interacting signaling pathways controlling multicellular development in Dictyostelium. *Curr. Opin. Genet. Develop*. **6,** 545–554.

Gerisch, G., Hülser, D., Malchow, D. & Wick, U. (1975). Cell communication by periodic cyclic-AMP pulses. *Phil. Trans. R. Soc. Lond. B* **272,** 181–192.

Hashimoto, Y., Cohen, M. H. & Robertson, A. (1975). Cell density dependence of the aggregation characteristics of the cellular slime mould Dictyostelium discoideum. *J. Cell Sci*. **19,** 215–229.

Höfer, T., Sherrat, J. A. & Maini, P. K. (1995). Cellular pattern formation during *Dictyostelium* aggregation. *Physica D* **85,** 425–444.

Kessler, D. A. & Levine, H. (1993). Pattern formation in *Dictyostelium* via the dynamics of cooperative biological entities. *Phys. Rev. E* **48,** 4801–4804.

Konijn, T. M. & Raper, K. B. (1961). Cell aggregation in Dictyostelium discoideum. *Dev. Biol*. **3,** 725–756.

Konijn, T. M. (1968) Chemotaxis in the cellular slime molds 2. The effect of density. *Biol. Bull*. **134,** 298–304.

Levine, H. & Reynolds, W. (1991). Streaming instability of aggregating slime mold amoebae. *Phys. Rev. Lett*. **66,** 2400–2403.

Levine, H., Aranson, I., Tsimring, I. & Truong, T. V. (1996). Positive genetic feedback governs cAMP spiral wave formation in Dictyotselium. *Proc. Natl. Acad. Sci. U.S.A*. **93,** 6382–6386.

Loomis, W. F. (1982). *The Development of Dictyostelium discoideum*. New York: Academic Press.

Mato, J. M., Losada, A., Nanjundiah, V. & Konijn, T. M. (1975). Signal input for a chemotactic response in the cellular slime mold Dictyostelium discoideum. *Proc. Natl. Acad. Sci. U.S.A*. **72,** 4991–4993.

Martiel, J. L. & Goldbeter, A. (1987). A model based on receptor desensitization for cAMP signaling in *Dictyostelium* cells. *Biophys. J*. **52,** 807–828.

Matsukuma, S. & Durston, A. J. (1979). Chemotactic cell sorting in Dictyostelium discoideum. *J. Embryol. Exp. Morphol*. **50,** 243–251.

Nanjundiah, V. (1973). Chemotaxis, signal relaying and aggregation morphology. *J. theor. Biol*. **42,** 63–105.

Parent, C. A. & Devreotes, P. N. (1996). Molecular genetics of signal transduction in *Dictyostelium*. *Annu. Rev. Biochem*. **65,** 411–440.

Parnas, H. & Segel, L. A. (1977). Computer evidence concerning the chemotactic signal in *Dictyostelium discoideum*. *J. Cell Sci*. **25,** 191–204.

Parnas, H. & Segel, L. A. (1978). A Computer study of pulsatile aggregation in *Dictyostelium discoideum*. *J. theor. Biol*. **71,** 185–207.

Rietdorf, J., Siegert, F. & Weijer, C. J. (1996). Analysis of wave propagation and cell movement during mound formation. *Dev. Biol*. **177,** 427–438.

Rietdorf, J., Siegert, F., Dharmawardhane, S., Firtel, R. A. & Weijer, C. J. (1997). Analysis of cell movement and signalling a constitutive active Gα1 subunit mutant of *Dictyostelium* discoideum defective in prestalk zone formation. *Dev. Biol*. **181,** 79–90.

Savill, N. J. & Hogeweg, P. (1997). Modelling morphogenesis: From single cells to crawling slugs. *J. theor. Biol*. **184,** 229–235.

Schaap, P., Tang, Y. H. & Othmer, H. G. (1996). A model for pattern formation *Dictyostelium* discoideum. *Differentiation* **60,** 1–16.

Siegert, F. & Weijer, C. J. (1989). Digital image processing of optical density wave propagation in *Dictyostelium discoideum* and the effects of caffeine and ammonia. *J. Cell Sci*. **93,** 325–335.

Siegert, F. & Weijer, C. J. (1991). Analysis of optical density wave propagation and cell movement in the cellular slime mould *Dictyostelium discoideum*. *Physica D* **49,** 224–232.

Siegert, F. & Weijer, C. J. (1995). Spiral and concentric waves organize multicellular *Dictyostelium* mounds. *Curr. Biol*. **5,** 937–943.

Steinbock, O., Siegert, F., Müller, S. C. & Weijer, C. J. (1993). Three-dimensional waves of excitation during *Dictyostelium* morphogenesis. *Proc. Natl. Acad. Sci. U.S.A*. **90,** 7332–7335.

Sternfeld, J. & David, C. N. (1981a). Cell sorting during pattern formation in *Dictyostelium discoideum*. *Differentiation* **20,** 10–21.

Sternfeld, J. & David, C. N. (1981b). Oxygen gradients cause pattern orientation in Dictyostelium cell clumps. *J. Cell Sci*. **50,** 9–17.

Tang, Y. H. & Othmer, H. G. (1995). Excitation, oscillations and wave propagation in a G-protein-based model of signal transduction in *Dictyostelium discoideum*. *Philos. Trans. R. Soc. Lond. Biol*. **349,** 179–195.

Tomchik, K. J. & Devreotes, P. N. (1981). Adenosine 3′, 5′-monophosphate waves in *Dictyostelium discoideum*: A demonstration by isotope dilution-fluorography. *Science* **212,** 443–446.

Tyson, J. J. & Keener, J. P. (1988). Singular perturbation theory of travelling waves in excitable media. *Physica D* **32,** 327–361.

Tyson, J. J. & Murray, J. D. (1989a). Cyclic AMP waves during aggregation of *Dictyostelium* amoebae. *Development* **106,** 421–426.

Tyson, J. J., Alexander, K. A., Manoranjan, V. S. & Murray, J. D. (1989b). Spiral waves of cyclic AMP in a model of slime mould aggregation. *Physica D* **34,** 193–207.

van Oss, C., Panfilov, A., Hogeweg, P., Siegert, F. & Weijer, C. J. (1996). Spatial pattern formation during the aggregation of the slime mould *Dictyostelium discoideum*. *J. theor. Biol*. **181**, 203–213.

Vasiev, B. N., Hogeweg, P. & Panfilov, A. V. (1994). Simulation of *Dictyostelium discoideum* aggregation via reaction-diffusion model. *Phys. Rev. Lett*. **73,** 3173–3176.

Vasiev, B., Siegert, F. & Weijer, C. J. (1997a). A hydrodynamic model for *Dictyostelium dictyostelium* mound formation. *J. theor. Biol*. **184,** 441–450.

Vasiev, B. Siegert, F. & Weijer, C. J. (1997b). Multi-armed spirals in excitable media. *Phys. Rev. Lett*. **78,** 2489–2492.

VASIEVA, O. O., VASIEV, B. N., KARPOV, V. A. & ZAIKIN, A. N. (1994). A model of *Dictyostelium discoideum* aggregation. *J. theor. Biol.* **171,** 361–367.

WILLIAMS, J. G. & JERMYN, K. A. (1991). Cell sorting and positional differentiation during Dictyostelium morphogenesis. In: *Cell-Cell Interactions in Early Development*. pp. 261–272. New York:.

WILLIAMS, J. (1995). Morphogenesis in *Dictyostelium*: New twists to a not-so-old tale. *Curr. Opin. Genet. Devel.* **5,** 426–431.